ring, on the other hand, may enhance the interconversions between the many helical forms of DNA. The pseudorotation of deoxyriboses in the DNA backbone remotely resembles the cis/trans peptide rotation that accompanies the I/II helical transformation in poly-L-proline. The distinctly different pseudorotation of the ribose and deoxyribose thus appears to be a general feature that characterizes the respective polynucleotides and that influences their recognition by various molecular agents.

Acknowledgment. We are grateful to Drs. Struther Arnott, Suse Broyde, Irena Ekiel, Michael Levitt, and Camillo Tosi for sharing unpublished data of relevance to this work, to Dr. Arnold Hagler for his critical evaluations of the project, and to a reviewer of this paper for drawing to our attention the recent related study of de Leeuw et al.[8] W.K.O. is also appreciative of the hospitality extended by Professor Joachim Seelig at the Biozentrum of the University of Basel, Switzerland, during the initial stages of this work and of a fellowship from the J.S. Guggenheim Memorial Foundation. This work was supported by grants from the U. S.P.H.S. (Grant GM-20861) and the Charles and Johanna Busch Memorial Fund of Rutgers University and the U.S./Israel Binational Science Foundation (1870/79). Computer time was supplied by the University of Basel Computer Center, The Weizmann Institute Computer Center, and the Rutgers University Center for Computer and Information Services.

Registry No. β-D-Ribofuranosylamine, 79681-15-5; β-D-erythro-deoxyribofuranosylamine, 79681-16-6.

Supplementary Material Available: Bibliographies of ribose and deoxyribose structures (Tables I-S and II-S) (12 pages). Ordering information is given on any current masthead page.

How Flexible Is the Furanose Ring? 2. An Updated Potential Energy Estimate

Wilma K. Olson

Contribution from the Department of Chemistry, Rutgers University, New Brunswick, New Jersey 08903. *Received November 25, 1980*

Abstract: A potential energy function is developed to estimate the pseudorotational motions of ribose and 2′-deoxyribose sugars. In addition to standard nonbonded, torsional, and valence angle strain contributions, an intrinsic gauche energy term is required to account for the puckering preferences and hindered ring flexibilities suggested by solid-state and solution studies. The gauche effect is also found to be an essential factor in reproducing the properties of 3′-deoxyribose and 2′-fluoro-2′-deoxyribose rings in solution. The extreme sensitvity of the potential energies to variations in ring geometry is helpful in understanding the disparities noted in 1 among earlier theoretical studies of furanose pseudorotation.[1] Apparently minor deviations of valence bond angles from standard X-ray values are found to perturb the normal motions of the furanose drastically.

Introduction

The inadequacy of theories to account satisfactorily for the physical properties of nucleic acids prompted the present reinvestigation of furanose pseudorotation. The comparative study detailed in the preceeding paper,[1] hereafter referenced as 1, reveals serious discrepancies between published potential energy surfaces and experimental observations of sugar puckering. No single potential method offered to date reproduces the unique conformational (puckering) preferences of different sugars (e.g., ribose and deoxyribose) and also mimics the known geometric (valence angle) changes that accompany furanose pseudorotation. Such discrepancies weaken the predictive value of theoretical work in bridging the gaps between experimental examples and also in extrapolating the behavior of low molecular weight nucleic acid analogues to long polynucleotide chains.

The difficulties in successful prediction of ribose and deoxyribose pseudorotation resemble conformational discrepancies found previously in several unrelated molecules constructed from the same chemical building blocks. The unexplained preference for certain pentose puckerings on the basis of steric and electrostatic forces alone parallels the anomalous predisposition of the O–C–C–C and O–C–C–O sequences in various polyoxides,[2,3] carbohydrates,[4-7] and smaller molecules[8-14] to adopt gauche in favor of trans rotational arrangements. This so-called "gauche" effect[15,16] characterizes a large assortment of compounds composed of atoms such as oxygen that possess unshared p electrons. According to quantum mechanical analyses,[17] the predisposition for gauche conformations in the aforementioned systems stems from stabilizing bond–antibond interactions involving the polar C–O linkages. The persistence of such effects in the furanose presumably influences the torsions of the five-membered ring and ultimately affects the potential energy of pseudorotation.

The computational improvements outlined below reconcile earlier discrepancies of semiempirical energy studies with the experimental properties of ribose and deoxyribose. The inclusion of gauche effects in the usual partitioned potential functions accounts at once for the unexplained puckering preferences of the different sugars. The extreme sensitivity of the potential energy function to internal ring geometry also helps to explain the disparities found in 1 among earlier theoretical estimates of pentose pseudorotation. Minor (2–3°) deviations of valence bond angles

(1) W. K. Olson and J. L. Sussman, *J. Am. Chem. Soc.*, preceding article in this issue.
(2) A. Abe and J. E. Mark, *J. Am. Chem. Soc.* **98**, 6468–6472 (1976).
(3) E. Riande and J. E. Mark, *Macromolecules*, **11**, 956–959 (1978).
(4) G. A. Jeffrey, J. A. Pople, and L. Radom, *Carbohydr. Res.*, **25**, 117–131 (1972); **38**, 81–95 (1974).
(5) A. Abe, *J. Am. Chem. Soc.*, **98**, 6477–6480 (1976).
(6) G. A. Jeffrey, J. A. Pople, J. S. Binkley, and S. Vishveshwara, *J. Am. Chem. Soc.*, **100**, 373–379 (1978).
(7) G. A. Jeffrey and R. Taylor, *J. Comput. Chem.*, **1**, 99–109 (1980).
(8) O. Bastiansen, *Acta Chem. Scand.*, **3**, 415–421 (1949).
(9) P. J. Krueger and H. D. Mettee, *J. Mol. Spectrosc.*, **18**, 131–140 (1965).
(10) P. Buckley and P. A. Giguère, *Can. J. Chem.*, **45**, 397–407 (1967).
(11) A. A. Abdurahmanov, R. A. Rahimova, and L. M. Imanov, *Phys. Lett. A*, **32A**, 123–124 (1970).
(12) H. Matsuura, M. Hiraishi, and T. Miyazawa, *Spectrochim. Acta, Part A*, **28A**, 2299–2304 (1972).
(13) L. Radom, W. A. Lathan, W. J. Hehre, and J. A. Pople, *J. Am. Chem. Soc.*, **95**, 695–698 (1973).
(14) W. K. Busfield, M. P. Ennis, I. J. McEwen, *Spectrochim. Acta, Part A*, **29A**, 1259–1264 (1973).
(15) E. L. Eliel and C. A. Giza, *J. Org. Chem.*, **33**, 3754–3758 (1968).
(16) S. Wolfe, *Acc. Chem. Res.*, **5**, 102–111 (1972).
(17) T. K. Brunck and F. Weinhold, *J. Am. Chem. Soc.*, **101**, 1700–1709 (1979).

0002-7863/82/1504-0278$01.25/0

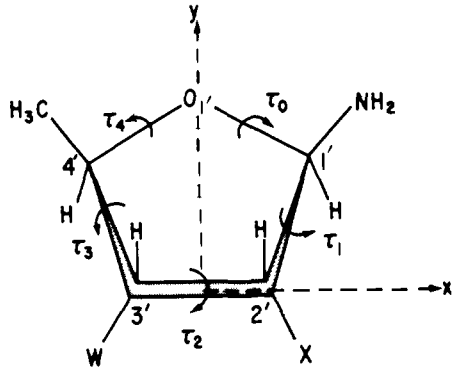

Figure 1. A schematic representation of the β-D-furanose ring of nucleic acids showing ring atoms, side groups, torsion angles, and coordinate axes (dashed lines). Systems treated here include ribose (W = X = OH), 2′-deoxyribose (W = OH, X = H), 3′-deoxyribose (W = H, X = OH), and 2′-fluoro-2′-deoxyribose (W = OH, X = F) with the base and 5′-CH_2OH of a nucleoside replaced by amino and methyl groups, respectively.

from standard X-ray values can lead, in some instances, to virtually "free" pseudorotation and, in other instances, to impossibly rigid motions compared to the limited ring flexibility consistent with solid-state and solution data.[1]

The set of optimal (structural and potential energy) parameters designed here to reproduce the known puckerings and geometries of ribose and deoxyribose specifically accounts as well for the unusual pseudorotation of 3′-deoxyribose and 2′-fluoro-2′-deoxyribose derivatives. The successful correlation of computation with observation in the latter systems enhances the predictive power of the present potential function and encourages its application to other molecules (such as the sugars in long oligo- and polynucleotides) not easily amenable to experimental study.

Pseudorotation States

The different puckerings along the pseudorotation cycle of furanose flexibility are described here, as in 1, in terms of the cooperative variations of the five ring torsion angles τ_j (j = 0–4 as in Figure 1). As illustrated by eq 1-1 (hereafter this designation means eq 1 from paper 1), each of the five torsion angles defining a given sugar puckering may be related to two parameters—τ_m, the maximum possible torsion angle, in degrees, in any of the different ring arrangements, and P, the relative phase angle displacement, in radians, of the specified puckered form from the $C_{2'}$-exo/$C_{3'}$-endo twist conformer as reference. A description of pseudorotation in terms of τ_m and P alone, however, is necessarily approximate since at least four independent parameters are required to specify the five ring torsion angles (cf. sequence). Despite this drawback, the τ_m/P description of pseudorotation originally offered by Altona and Sundaralingam[18] is conceptually very simple and is easily related to molecular observations.

Alternatively, the conformational variations on the pseudorotation circuit may be expressed indirectly in terms of the cooperative out-of-phase vibrations z_i (i = 0–4 where i = 0 is $O_{1'}$, i = 1 is $C_{1'}$, etc.) of a planar five-membered ring.[19] The z_i are described with respect to a uniquely defined mean plane such that $\sum_i z_i = \sum_i z_i \cos 0.4\,\pi(i-1) = \sum_i z_i \sin 0.4\,\pi(i-1) = 0$ together with amplitude (q) and phase angle (Ψ) parameters analogous to τ_m and P. Because of the judicious choice of the mean plane, the q/Ψ description of ring puckering is mathematically exact and is usually preferred in the extraction of pseudorotation parameters from crystallographic data.[20] The q/Ψ approach, however, is less useful in studies such as the present that attempt to generate theoretical structures with standard geometries. In view of the stringent constraints placed upon structural variables in model furanoses, it is more appropriate to generate conformers directly by using the τ_m/P approximation rather than to extract structural details indirectly from the exact q/Ψ relationships.

Pentose Geometry

The three-dimensional spatial configuration of a given furanose puckering is described here directly in terms of the internal geometry (bond lengths and valence angles) and bond rotations of the five-membered ring. Until now, theoretically puckered rings were generated in terms of various artificial parameters such as the rectilinear displacements of ring atoms from a suitably chosen mean plane[19,21] or the curvilinear displacements of these atoms from a specific planar segment of the pentose[22] that only indirectly describe the geometrical features of the ring. As noted in 1, the valence angle variations that result upon energy minimization in these rings are usually widely discrepant from solid-state observations. The endocyclic valence bond angles of the furanose are known from crystallographic studies to vary in a sinusoidal fashion with the phase angle of pseudorotation P.[23,24]

Owing to constraints of ring closure, it is necessary in describing the pentose configuration to specify only nine of its fifteen structural parameters (e.g., the five bond lengths l, the five valence bond angles θ, and the five torsion angles τ).[21] Moreover, since the bond lengths may be regarded in good approximation as fixed,[25] it is necessary to specify only four of the ten remaining variables. In order to match the known fluctuations in furanose geometry most easily, it is appropriate to choose the valence angles at the four carbon atoms as independent structural variables.

For the purpose of generating molecular coordinates, a right-handed Cartesian coordinate system is constructed in the plane defined by atoms $C_{2'}$, $C_{3'}$, and $O_{1'}$ (see the model pentose in Figure 1). The x axis is chosen to lie along the $C_{2'}$–$C_{3'}$ bond vector, and the y axis is defined by the perpendicular drawn from $O_{1'}$ to the x axis. The atomic coordinates of $C_{2'}$, $C_{3'}$, and $O_{1'}$ in this system are thus given by

$$\mathbf{v}_{C_{2'}} = (a, 0, 0) \qquad \mathbf{v}_{C_{3'}} = (-b, 0, 0) \qquad \mathbf{v}_{O_{1'}} = (0, c, 0)$$

where the distances a, b, and c are simple functions of ring geometry (i.e., $a = (l_{CC} - 2l_{CO}(\cos\theta^{C_{1'}} - \cos\theta^{C_{4'}}))/2$, $b = l_{CC} - a$, and $c = (l_{CC}^2 + l_{CO}^2 - 2l_{CC}l_{CO}\cos\theta^{C_{1'}} - a^2)^{1/2}$) and where l_{CC} and l_{CO} are the fixed lengths of the C–C and C–O bonds, respectively. A superscript is used to identify the endocyclic valence angles centered at $C_{1'}$ and $C_{4'}$.

The six positional parameters of the $C_{1'}$ and $C_{4'}$ atoms in the above coordinate frame may then be found from the six equations given in eq 1 that reflect the structural constraints placed upon the cyclic system.

$$(\mathbf{v}_{O_{1'}} - \mathbf{v}_{C_{1'}})\cdot(\mathbf{v}_{C_{2'}} - \mathbf{v}_{C_{1'}}) = l_{CO}l_{CC}\cos\theta^{C_{1'}}$$

$$(\mathbf{v}_{C_{1'}} - \mathbf{v}_{C_{2'}})\cdot(\mathbf{v}_{C_{3'}} - \mathbf{v}_{C_{2'}}) = l_{CC}^2\cos\theta^{C_{2'}}$$

$$(\mathbf{v}_{C_{2'}} - \mathbf{v}_{C_{3'}})\cdot(\mathbf{v}_{C_{4'}} - \mathbf{v}_{C_{3'}}) = l_{CC}^2\cos\theta^{C_{3'}}$$

$$(\mathbf{v}_{C_{3'}} - \mathbf{v}_{C_{4'}})\cdot(\mathbf{v}_{O_{1'}} - \mathbf{v}_{C_{4'}}) = l_{CO}l_{CC}\cos\theta^{C_{4'}}$$

$$(\mathbf{v}_{O_{1'}} - \mathbf{v}_{C_{1'}})\cdot[(\mathbf{v}_{C_{3'}} - \mathbf{v}_{C_{2'}}) \times (\mathbf{v}_{C_{2'}} - \mathbf{v}_{C_{1'}})] = l_{CO}l_{CC}^2\sin\tau_1\sin\theta^{C_{1'}}\sin\theta^{C_{2'}}$$

$$(\mathbf{v}_{O_{1'}} - \mathbf{v}_{C_{4'}})\cdot[(\mathbf{v}_{C_{3'}} - \mathbf{v}_{C_{2'}}) \times (\mathbf{v}_{C_{4'}} - \mathbf{v}_{C_{3'}})] = l_{CO}l_{CC}^2\sin\tau_3\sin\theta^{C_{3'}}\sin\theta^{C_{4'}} \quad (1)$$

The dot and cross symbols are used to denote dot or scalar and cross or vector products, respectively. The τ_1 and τ_3 torsion angles appearing in eq 1 and also designated in Figure 1 are obtained from the four independent valence angles as indicated by eq 2.

(18) C. Altona and M. Sundaralingam, *J. Am. Chem. Soc.*, **94**, 8205–8212 (1972).
(19) D. Cremer and J. A. Pople, *J. Am. Chem. Soc.*, **97**, 1358–1367 (1975).
(20) G. A. Jeffrey and R. Taylor, *Carbohydr. Res.*, **81**, 182–183 (1980).
(21) J. D. Dunitz, *Tetrahedron*, **28**, 5459–5467 (1972).
(22) V. Sasisekharan in "The Jerusalem Symposia on Quantum Chemistry and Biochemistry", Vol. 5, E. D. Bergmann and B. Pullman, Eds., The Israel Academy of Sciences and Humanities, Jerusalem, 1973, pp 247–260.
(23) P. Murray-Rust and S. Motherwell, *Acta Crystallogr., Sect. B*, **B34**, 2534–2546 (1978).
(24) E. Westhof and M. Sundaralingam, *J. Am. Chem. Soc.*, **102**, 1493–1500 (1980).
(25) S. Arnott, S. D. Dover, and A. J. Wonacott, *Acta Crystallogr. Sect. B*, **B25**, 2192–2206 (1969).

$$\cos \tau_1 = (l_{CC}(1 - 2\cos \theta^{C_2'}) + 2l_{CO}(\cos \theta^{C_4} - (1 - \cos \theta^{C_2'}) \cos \theta^{C_1'}))/2l_{CO} \sin \theta^{C_1'} \sin \theta^{C_2'}$$

$$\cos \tau_3 = (l_{CC}(1 - 2\cos \theta^{C_3'}) + 2l_{CO}(\cos \theta^{C_1'} - (1 - \cos \theta^{C_3'}) \cos \theta^{C_4'}))/2l_{CO} \sin \theta^{C_3'} \sin \theta^{C_4'} \quad (2)$$

The torsional parameters are defined, following Altona and Sundaralingam,[18] relative to a cis = 0° reference conformation with positive values assigned to right-handed rotations. Once the ring coordinates are specified with eq 1, the $\theta^{O_1'}$ valence angle and the τ_0, τ_2, and τ_4 ring torsions may be computed by using relationships analogous to those given above.

Atomic coordinates may additionally be assigned to the protons H and heavy atoms A attached to the ring carbons C_j of the $C_i - C_j - C_k$ ring sequences. For simplicity, it is assumed that all valence angles involving the protons are tetrahedral and all C–H bonds are 1 Å long so that for the general case

$$(\mathbf{v}_{C_i} - \mathbf{v}_{C_j})\cdot(\mathbf{v}_H - \mathbf{v}_{C_j}) = -l_{CC}/3$$

$$(\mathbf{v}_{C_k} - \mathbf{v}_{C_j})\cdot(\mathbf{v}_H - \mathbf{v}_{C_j}) = -l_{CC}/3$$

$$(\mathbf{v}_A - \mathbf{v}_{C_j})\cdot(\mathbf{v}_H - \mathbf{v}_{C_j}) = -l_{AC}/3$$

$$(\mathbf{v}_H - \mathbf{v}_{C_j})\cdot[(\mathbf{v}_{C_k} - \mathbf{v}_{C_j}) \times (\mathbf{v}_{C_i} - \mathbf{v}_{C_j})] = -l_{CC}^2[9 - 2(1 + \cos \theta^{C_j})]^{1/2} \sin \theta^{C_j}/3 \quad (3)$$

Furthermore, the side group A is presumed to occupy a symmetrical position with respect to the neighboring ring atoms C_i and C_k such that the valence angles A–C_j–C_i and A–C_j–C_k are equivalent and are given by the parameter ν.

$$(\mathbf{v}_{C_i} - \mathbf{v}_{C_j})\cdot(\mathbf{v}_A - \mathbf{v}_{C_j}) = l_{C_iC}l_{AC} \cos \nu$$

$$(\mathbf{v}_{C_k} - \mathbf{v}_{C_j})\cdot(\mathbf{v}_A - \mathbf{v}_{C_j}) = l_{CC_k}l_{AC} \cos \nu$$

$$(\mathbf{v}_A - \mathbf{v}_{C_j})\cdot[(\mathbf{v}_{C_k} - \mathbf{v}_{C_j}) \times (\mathbf{v}_{C_i} - \mathbf{v}_{C_j})] = l_{C_iC}l_{CC_k}l_{AC}[1/\cos^2 \nu - 2(1 + \cos \theta^{C_j})]^{1/2} \sin \theta^{C_j} \cos \nu \quad (4)$$

Atomic coordinates obtained by this procedure for the model ribose sugar illustrated in Figure 1 are reported for twenty puckered states ($P = 0$ to 1.9π rad at 0.1π-rad increments, $\tau_m = 38°$) in Table I-S of the supplementary material. These particular structures are found below to possess the lowest potential energies (cf. sequence) of the many different three-dimensional arrangements that are described by each given combination of P and τ_m.

Potential Energy Functions

The conformational energies of the differently puckered furanose molecules constructed here reflect the combined contributions of nonbonded interactions (V_{NB}), valence angle strain (V_{STR}), intrinsic torsional barriers (V_{TOR}), and gauche effects (V_G).

$$V(P, \tau_m) = V_{NB} + V_{STR} + V_{TOR} + V_G \quad (5)$$

Each conformer described below additionally satisfies a pseudorotational constraint energy (V_{PSEU}, in kcal/mol) of the form

$$V_{PSEU} = \sum_{j=0}^{4} 1000(1 - \cos (\tau_j - \tau_j^0)) \quad (6)$$

where the τ_j are the actual ring torsion angles of the structure and the τ_j^0 are the ideal torsion angles predicted by eq 1–1 for a particular choice of P and τ_m. This artificial potential, introduced originally by Levitt and Warshel,[26] gives rise to very large energies when the τ_j differ by only a few degrees from the τ_j^0 and thus forces the five-membered ring to follow a particular pseudorotational path. Because the V_{PSEU} contribution is negligible and virtually constant (0.2–0.4 kcal/mol) upon variation of P and τ_m, we do not include V_{PSEU} in the total $V(P, \tau_m)$ values reported below for each puckering.

(26) M. Levitt and A. Warshel, *J. Am. Chem. Soc.*, **100**, 2607–2613 (1978).

Table I. Parameters for Nonbonded Interactions

atom or group	α, Å^3	N	r^0, Å
H	0.42	0.9	1.3
C	0.93	5	1.8
O	0.64	7	1.6
CH_3	1.77	7	2.0
NH_2	1.87	8	2.0
OH	1.06	8	1.7
F	0.64	8	1.5

Table II. Comparative Electronic Charge Distributions[a]

atom or group	ribose (W = X = OH)[b]	2′-deoxyribose (W = OH, X = H)	3′-deoxyribose (W = H, X = OH)	2′-fluoro-2′-deoxyribose (W = OH, X = F)
$O_{1'}$	−0.271	−0.271	−0.271	−0.271
$C_{1'}$	0.127	0.114	0.127	0.127
NH_2-1′	−0.053	−0.053	−0.053	−0.053
$H_{1'}$	0.051	0.051	0.051	0.051
$C_{2'}$	0.107	−0.041	0.076	0.129
$X_{2'}$	−0.157	0.042	−0.157	−0.179
$H_{2'}$	0.052	0.042	0.052	0.052
$C_{3'}$	0.105	0.077	−0.041	0.105
$W_{3'}$	−0.155	−0.155	0.042	−0.155
$H_{3'}$	0.052	0.052	0.042	0.052
$C_{4'}$	0.094	0.094	0.084	0.094
CH_3-4′	−0.003	−0.003	−0.003	−0.003
$H_{4'}$	0.051	0.051	0.051	0.051

[a] Charges expressed in esu. [b] See Figure 1 for the locations of W and X.

The V_{NB} term appearing in eq 5 includes the London attractions, van der Waals repulsions, and Coulombic interactions between all pairs of nonbonded atoms or heavy atom groups (e.g., CH_3, NH_2, and OH) separated by at least three intervening chemical bonds. Pairs of atoms separated by three internal bonds of the furanose ring, however, do not contribute to the nonbonded potential. Instead, we consider the interactions between ring atoms in the V_{STR} term outlined below.

The parameters (α, N, r^0, and δ) adopted to describe the nonbonded interactions between the various atoms and "point" groups in standard V_{NB} expressions[27] are listed in Tables I and II. The values of α, N, and r^0 assigned in Table I to carbon, fluorine, hydrogen, oxygen, and methyl are data used previously in analyses of alkanes,[28] peptides,[29,30] polyoxides,[2] pyranosides,[5] and fluorocarbons.[31] For consistency, the amino and hydroxyl parameters introduced here are derived in a manner similar to those used in the earlier studies.[2,5,28-31] The atomic polarizabilities α and the effective numbers of valence electrons N are combined by using the Slater–Kirkwood equation[28] to evaluate pairwise constants of the London dispersion energy, while the van der Waals radii r^0 are utilized to determine the pairwise constants of the van der Waals repulsive interactions. The sum of r^0 values associated with each pairwise interaction is equal to the distance at which the combined London and van der Waals energies of the pair is a minimum. The values of r^0 listed in Table I are slightly larger than van der Waals radii deduced from crystallographic data[32] for reasons detailed elsewhere.[30]

The list of partial charges given in Table II is required to evaluate the pairwise Coulombic energies in the different sugars. These data are based upon the approximate charge distributions used originally by Davis[33] for ribose and 2′-deoxyribose. The

(27) W. K. Olson and P. J. Flory, *Biopolymers*, **11**, 25–56 (1972).
(28) K. S. Pitzer, *Adv. Chem. Phys.*, **2**, 59–83 (1959).
(29) D. A. Brant and P. J. Flory, *J. Am. Chem. Soc.*, **87**, 2791–2800 (1965).
(30) D. A. Brant, W. G. Miller, and P. J. Flory, *J. Mol. Biol.*, **23**, 47–65 (1967).
(31) T. W. Bates, *Trans. Faraday Soc.*, **63**, 1825–1834 (1967).
(32) A. Bondi, *J. Chem. Phys.*, **68**, 441–451 (1964).

partial charges accorded the chemical groups are given by the sums of the δ's assigned previously to the sets of constituent atoms. Furthermore, the distribution of charges in the vicinity of $C_{3'}$ in 3'-deoxyribose is presumed to resemble that found about $C_{2'}$ in 2'-dexoyribose. The partial charges of 0.129 and −0.179 at $C_{2'}$ and $F_{2'}$ in 2'-fluoro-2'-deoxyribose are chosen to reproduce the known dipole of 1.2 D[31] associated with the C–F bond and also to satisfy the requirements of electroneutrality. A dielectric constant ϵ of 4.0 is introduced in the Coulombic potential to conform with observed measurements on model glycosides.[34]

The endocyclic and exocyclic valence angle strain V_{STR} that accompanies puckering of the furanose ring is accounted for by a sum of harmonic bond angle bending terms of the form

$$V_{STR} = K_\theta(\theta - \theta^0)^2$$

In this expression K_θ is the force constant, θ the observed valence angle (in radians), and θ^0 the ideal rest or equilibrium value of the particular angle. The θ^0 are taken to be tetrahedral (1.91 rad) for the all valence angles of the furanose. Since the valence angles involving hydrogen are assumed to be tetrahedral, only heavy-atom sequences are included in V_{STR}. The K_θ are estimated, following Levitt and Warshel,[26] to be 40, 34, and 30 kcal/(mol rad^2) for C–O–C, C–C–O, and C–C–C sequences, respectively. These values are approximately 40% of the force constants reported by Snyder and Zerbi[35] in studies of aliphatic ethers and only 20% of those obtained by Eyster and Prohofsky[36] in a normal coordinate analysis of poly(rA) and poly(rU). Upon energy minimization, the larger force constants are found by us (in calculations to be detailed elsewhere) to describe furanose geometries in considerable disagreement with relevant solid-state examples.[23,24]

The V_{TOR} term is included in eq 5 to take account of the more subtle contributions from bond orbitals associated with the atoms attached to a given bond,[29,37,38] including the effects of distortion of these orbitals by rotation.[39] The potential is taken to be threefold for the five torsions of the pentose ring and is represented by a term of the form

$$V_{TOR} = \sum_{j=0}^{4} (V_3/2)(1 + \cos 3\tau_j)$$

Barrier heights V_3 of 2.8 and 1.8 kcal/mol are assigned to rotations centered about C–C and C–O bonds, respectively. These values are chosen to reproduce the observed barrier heights of *n*-propyl fluoride (2.69–2.87 kcal/mol),[40] butane (3.5 kcal/mol),[41-44] and methyl ethyl ether (2.53 kcal/mol)[40] when V_{TOR} is used in combination with the V_{NB} potential reported above.

The intrinsic tendency of selected atomic sequences to favor gauche in preference to trans conformations is modeled by a phenomenological gauche potential of the form

$$V_G = \sum_{i=1}^{m} (V_2/2)(1 + \cos 2\phi_i) \qquad (7)$$

When used alone, such a term is found to favor perpendicular (±90°) conformation angles over either trans (180°) or cis (0°) states. When used in combination with a standard threefold torsional potential, however, the V_G term is able to account for experimentally known trans/gauche (t/g) energy differences.[45] The ϕ_i rotations appearing in eq 7 are related by phase angle shifts (of approximately 0 or ±120°) to the ring torsion angles (τ) sharing common central bonds. More than one ϕ may be associated with a particular τ_j so that the number of gauche contributions m is usually an integer greater than 5. For example, associated with the $C_{1'}$–$C_{2'}$–$C_{3'}$–$C_{4'}$ τ_2 rotation in ribose are three ϕ rotations about $C_{1'}$–$C_{2'}$–$C_{3'}$–$O_{3'}$, $O_{2'}$–$C_{2'}$–$C_{3'}$–$O_{3'}$, and $O_{2'}$–$C_{2'}$–$C_{3'}$–$C_{4'}$. Barrier heights V_2 of 0.2, 1.0, 0.3, and 2.8 kcal/mol are introduced to reproduce the known trans/gauche energy differences in O–C–C–C,[2,5] O–C–C–O,[2] F–C–C–C,[46] and F–C–C–O[47] bond fragments, respectively. A similar gauche term for the O–C–C–O linkage was derived independently by Marsh et al.[48] in recent theoretical calculations on cyclic nucleotides. V_G expressions analogous to eq 7 have also been used previously in theoretical treatments of the phosphodiester rotations of the polynucleotides.[49,50]

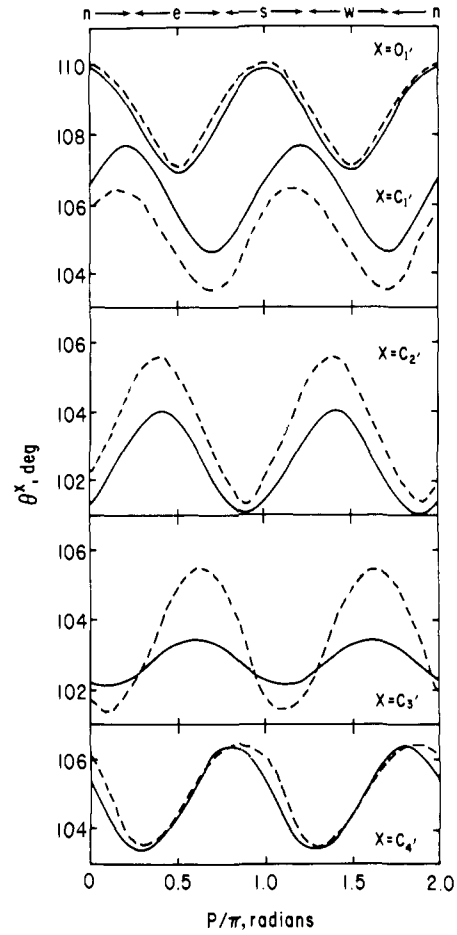

Figure 2. Comparative pseudorotational variations of endocyclic valence angles θ^X of furanose rings associated with energy optimization in this work (dashed curves) and observed in X-ray crystallographic regression (RGN) analyses (solid lines).[23,24] The four quadrants (n, e, s, w) of pseudorotation space associated wtih the major categories of sugar puckering are noted above the figure.

(33) R. C. Davis, Ph.D. Thesis, University of California, Berkeley, California, 1967.
(34) C. P. Smyth, "Dielectric Constant and Molecular Structure", The Chemical Catalog Company, Inc., New York, 1931.
(35) R. G. Synder and G. Zerbi, *Spectrochim. Acta, Part A*, **23A**, 391–437 (1967).
(36) J. M. Eyster and E. W. Prohofsky, *Biopolymers*, **13**, 2505–2526 (1974).
(37) R. A. Scott and H. A. Scheraga, *J. Chem. Phys.*, **42**, 2209–2215 (1965).
(38) I. R. Epstein and W. N. Lipscomb, *J. Am. Chem. Soc.*, **92**, 6094–6095 (1970).
(39) W. L. Jorgensen and L. C. Allen, *J. Am. Chem. Soc.*, **93**, 567–574 (1971).
(40) D. R. Herschbach, "Bibliography for Hindered Internal Rotation and Microwave Spectroscopy", Lawrence Radiation Laboratory, University of California, Berkeley, California, 1962.
(41) K. S. Pitzer, *Ind. Eng. Chem.*, **36**, 829–831 (1944).
(42) W. B. Person and G. C. Pimental, *J. Am. Chem. Soc.*, **75**, 532–538 (1953).
(43) K. S. Pitzer, *J. Am. Chem. Soc.*, **63**, 2413–2418 (1941).
(44) B. P. Dailey and W. A. Felsing, *J. Am. Chem. Soc.*, **65**, 44–46 (1943).
(45) If the trans and gauche$^\pm$ conformations of a particular bond rotation are located at rotational isomeric states of 180° and ±60°, respectively, the trans/gauche energy difference is given simply by $(V_3/2)[(1 + \cos 540°) - (1 + \cos \pm 180°)] + (V_2/2)[(1 + \cos 360°) - (1 + \cos \pm 120°)] = 3V_2/4$. A somewhat more complicated expression can be derived in an analogous fashion when each of the rotational domains spans a broad range of angular values.
(46) J. R. Lacher and H. A. Skinner, *J. Chem. Soc. A*, 1034–1038 (1968).
(47) K. Hagen and K. Hedberg, *J. Am. Chem. Soc.*, **95**, 8263–8266 (1973).
(48) F. J. Marsh, P. Weiner, J. E. Douglas, P. A. Kollman, G. L. Kenyon, and J. A. Gerlt, *J. Am. Chem. Soc.*, **102**, 1660–1665 (1980).
(49) G. Govil, *Biopolymers*, **15**, 2303–2307 (1976).

Conformational Energies

Optimized Geometries. The total conformational energy described by eq 5 was computed at increments of 0.1π rad from $P = 0$ to 1.9π rad for a series of puckered structures along the $\tau_m = 38°$ cycle of furanose pseudorotation. Each of the puckered conformers was constructed following eq 1 and 2 in terms of the geometric parameters of the ring. The C–O and C–C bond lengths were fixed respectively at values of 1.435 and 1.52 Å while the internal carbon-centered (θ^C) valence angles were varied at increments of either 2° or 0.5° between 98° and 108°. The ring torsion angles and the endocyclic $O_{1'}$ valence angle were then determined from the computed ring coordinates. Side group and proton substituents were next added to the basic ring structures matching the torsion angle (i.e., pseudorotation) constraints of eq 6. The heavy-atom side groups were separated from the ring carbons by C–C, C–N, C–O, and C–F bonds of 1.51, 1.47, 1.43, and 1.40 Å, respectively, in length. Finally, the completed molecular models were compared on the basis of total energy $V(P, \tau_m)$ and the optimal puckered forms chosen.

The set of endocyclic valence angles associated with the energetically optimized furanose molecules are plotted as functions of P in Figure 2 (dashed lines). The data are compared with regression (RGN) curves (solid lines) determined for each angle on the basis of available crystallographic data.[23,24] The theoretical variations are seen to match the RGN curves much more closely than the previous theoretical predictions reported in Figures 5–7 of 1. The data obtained here are almost completely in phase with the experimentally generated curves. The magnitudes of the theoretical and experimental angular fluctuations in Figure 2 are roughly comparable for all valence angles except $\theta^{C_{3'}}$. The theoretical increase of this angle in the e and w quadrants of pseudorotation space (noted at the top of Figure 2) is approximately triple that of the corresponding RGN curve. It is notable, however, that the major uncertainty in all the RGN curves occurs in the e- and w-puckered domains where there are few, if any, experimental examples. The segments of the RGN curves in these regions may very likely be modified as more e- and w-type crystal structures are solved. The theoretical predictions of all five endocyclic angles, however, are found to match the RGN curves very closely in the highly populated (and better characterized) n and s quadrants of sugar puckering. Nevertheless, because of the structural symmetry imposed by our choice of fixed bond lengths, the computed variations of $\theta^{C_{3'}}$ are equivalent to those determined for $\theta^{C_{2'}}$. The experimental variations of $\theta^{C_{3'}}$ in Figure 2 are probably smaller than those of $\theta^{C_{2'}}$ in view of the known (~0.04 Å) shortening of $O_{1'}$–$C_{1'}$ compared to $C_{4'}$–$O_{1'}$ in numerous crystal structures.[25,51] Unfortunately, this difference in bond lengths is not able to account for the large difference in the theoretical and RGN values of $\theta^{C_{3'}}$ observed here. When the $O_{1'}$–$C_{1'}$ bond length is decreased from 1.435 to 1.395 Å, for example, the theoretical value of $\theta^{C_{3'}}$ at $P = 0.7\pi$ rad is decreased from 105.3 to only 104.1°. The value of 103.3° associated with the RGN curve at this point may therefore reflect the bias of the limited experimental data.

Ribose. Curves associated with the various contributions to the pseudorotational energy of our model ribose are reported in Figure 3. The data are plotted as relative energies vs. the pseudorotational phase angle P. Normalized statistical weights based on the total energy of the system are illustrated by the bar graph above the diagram. The preferred domains of the model are seen at once to be the n- and s-puckered states observed in most solid-state studies. (For comparison, see Table 1-I). Furthermore, these two puckering categories are approximately equally favored, the relative statistical weights σ_n and σ_s based upon eq 1-4 being 0.48 and 0.51, respectively. The intermediate e and w domains, however, are passed through very rapidly, the n–e–s pseudorotational path (where $\sigma_e = 0.01$) being considerably more preferred than the s–w–n route ($\sigma_w = 0.0004$).

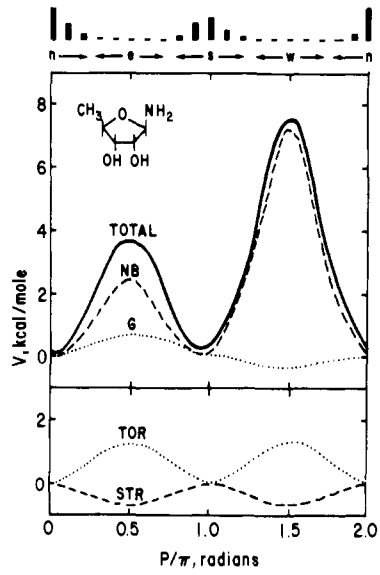

Figure 3. The computed relative variations of the total potential energy V and its various energy components in kcal/mol as a function of the pseudorotation phase angle (P) of ribose. Normalized statistical weights σ based upon the total energy of the system and quadrants of pseudorotation space are represented at the top of the diagram.

As evident from Figure 3, the major contribution to the pseudorotational potential of ribose comes from the nonbonded interactions (V_{NB}) between the side groups attached to the five-membered ring. The local energy maxima at $P = 0.5\pi$ and 1.5π rad primarily reflect the repulsive van der Waals forces between the (eclipsed) 2′- and 3′-hydroxyl groups of the molecule. The higher energy barrier at $P = 1.5\pi$ rad stems from additional close steric contacts involving the methyl group attached to $C_{4'}$ and the amino group linked to $C_{1'}$ in this puckered state. In agreement with previous reports by Levitt and Warshel,[26] electrostatic interactions as monitored by a pairwise Coulombic potential play little role in the determination of the nonbonded energies in Figure 3. The total Coulombic energy term varies by less than 0.25 kcal/mol over the entire pseudorotation cycle.

The strain of valence angle deformations (V_{STR}) in the ribose ring is the only contribution to the total pseudorotational potential in Figure 3 that clearly favors the e- and w-puckering domains over the n and s ranges. From Figure 2 it is evident that the endocyclic valence angles as a whole are closer to ideal tetrahedral geometry ($\theta^0 = 109.47°$) at $P = 0.5\pi$ and 1.5π rad than at 0 and π rad. As noted previously by Levitt and Warshel,[26] the intrinsic torsional energy (V_{TOR}) of rotations about the five ring bonds is greatest in the e and w domains when the conformations about the C–C single bonds (which possess higher barrier heights than the C–O single bonds) are maximally eclipsed. According to Figure 3 the n and s states at 0 and π rad, respectively, are favored over the e conformer at 0.5π rad by approximately 1.3 kcal/mol of intrinsic torsional energy.

The gauche contribution to the potential energy of ribose is determined principally by the three O–C–C–O sequences of the molecule. (The V_2 barrier height of eq 7 is much greater for O–C–C–O than for O–C–C–C interactions.) The V_G term is accordingly greatest in the e domain when two of the three O–C–C–O rotations ($O_{1'}\cdots O_{2'}$ and $O_{1'}\cdots O_{3'}$) are trans and lowest in the w range when two of the three (again $O_{1'}\cdots O_{2'}$ and $O_{1'}\cdots O_{3'}$) are gauche. In n- and s-puckered sugars only one of the aforementioned two angles is gauche with the other trans. The $O_{2'}$–$C_{2'}$–$C_{3'}$–$O_{3'}$ rotation is found in a highly unfavored cis arrangement at $P = 0.5\pi$ and 1.5π rad that is only partially relieved upon pseudorotation to n and s states. The net effect of the gauche interactions in ribose, then, is to raise the torsional barrier of e-puckered sugars and to lower that of w-puckered systems compared to equally favored n and s domains.

2′-Deoxyribose. According to Figure 4 the substitution of the large 2′-hydroxyl of ribose by a small proton in deoxyribose not

(50) D. M. Hayes, P. A. Kollman, and S. Rothenberg, *J. Am. Chem. Soc.*, **99**, 2150–2154 (1977).
(51) M. Sundaralingam, *J. Am. Chem. Soc.*, **87**, 599–606 (1965).

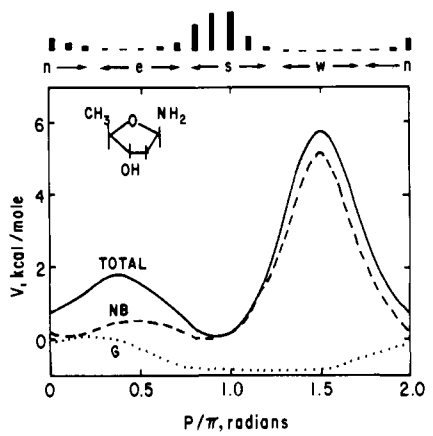

Figure 4. Variation of the total and constituent (nonbonded and gauche) energies in kcal/mol as a function of the pseudorotation of 2′-deoxyribose. See legend to Figure 3.

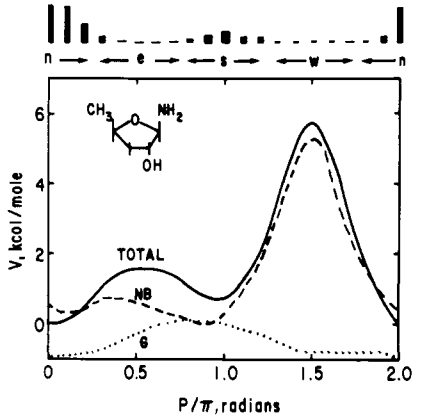

Figure 5. Variation of the total and constituent (nonbonded and gauche) energies in kcal/mol as a function of the pseudorotation of 3′-deoxyribose. See legend to Figure 3.

only lowers the barrier to pseudorotation but also shifts the distribution of n and s conformers. In our model system the s quadrant of pseudorotation space with $\sigma_s = 0.74$ assumes major importance compared to all other domains. As outlined in 1, no previous theoretical study matches the observed distribution of X-ray data ($\sigma_s = 0.67$) so closely as this. In contrast to the X-ray values, however, the predicted population of the e quadrant in Figure 4 ($\sigma_e = 0.11$) nearly matches that in the n quadrant ($\sigma_n = 0.15$). In the 11 currently available crystal structures of n- and e-puckered deoxyriboses, the n conformers outnumber the e by more than 2:1 (see Table 1–II). The present calculations, nevertheless, confirm the suggestion from X-ray studies[18] that the pseudorotation of deoxyribose is hindered. The energy barrier of 1.8 kcal/mol at $P = 0.4\pi$ rad, while low enough to permit interconversion of sugar puckering, prevents "free" pseudorotational motions along the n–e–s path. The additional barrier of 5.8 kcal/mol at $P = 1.5\pi$ rad hinders the motions of the ring along the s–w–n path even further.

As in ribose, nonbonded interactions persist as the major determinant of the total pseudorotational energy of w-puckered deoxyriboses. According to Figure 4, however, the V_{NB} contributions diminish to negligible levels in e-puckered structures. The van der Waals repulsions between the eclipsed 2′-proton and 3′-hydroxyl of deoxyribose increase the energy at $P = 0.5\pi$ rad by less than 0.5 kcal/mol above the two nearly equivalent energy minima at $P = 0.1\pi$ and 0.9π rad. The Coulombic interactions fluctuate less than 0.05 kcal/mol over this range.

If only nonbonded contributions are considered, the deoxyribose behaves as a freely pseudorotating ring. The additional contributions of V_{STR} and V_{TOR} raise the energy slightly so that the e domain then lies about 1.0 kcal/mol above the n and s ranges. The interconversion between n and s states, however, hardly classifies as hindered motion on this basis. Furthermore, the combination of V_{NB}, V_{STR}, and V_{TOR} does not explain the decided preference for s puckering in deoxyribose crystal structures. Because the V_{STR} and V_{TOR} energies of deoxyribose are equivalent to those reported in Figure 3 for ribose, they do not appear in Figure 4.

As seen in Figure 4, the structural asymmetry of the deoxyribose molecule is also reflected in the gauche contribution to the total pseudorotational energy. The V_G term of deoxyribose is governed primarily by the $O_{1'}$–$C_{4'}$–$C_{3'}$–$O_{3'}$ torsional sequence. This interaction is greatest in n-puckered sugars when the angle is trans and lowest in s-puckered sugars when the angle is gauche. As with the V_G term for ribose, the intermediate e quadrant is somewhat disfavored on this basis compared to the w range. Indeed, this final contribution to the total potential energy is what is necessary to account for the apparently hindered pseudorotation of deoxyribose in experimental studies. More importantly, the gauche energy is the only contribution to the potential in Figure 4 that can mimic the long observed preference for s-type ($C_{2'}$-endo) ring puckering in deoxyribose.

3′-Deoxyribose. The extension of the present potential energy methods to 3′-deoxyribose or cordycepin, an antibiotic that inhibits bacterial and mammalian cell growth,[52,53] immediately explains its known preference for n-type puckering.[54–57] According to Figure 5, n-puckered sugars predominate over s-puckered sugars by a margin of $\sigma_n = 0.69$ to $\sigma_s = 0.20$. The e-type sugars with $\sigma_e = 0.11$ occur to the same extent as in 2′-deoxyribose. The potential energy barriers to pseudorotation for 3′-deoxyribose also resemble those reported above for 2′-deoxyribose. The total potential barrier at $P = 0.6\pi$ rad in the e quadrant equals 1.6 kcal/mol and at $P = 1.5\pi$ rad in the w quadrant, 5.8 kcal/mol.

According to Figure 5, s-type puckering is slightly favored (by 0.3 kcal/mol) over n-type puckering on the basis of the nonbonded interactions of 3′-deoxyribose. Like that found above for 2′-deoxyribose, the intermediate e quadrant is also relatively favored by the nonbonded term. In both deoxyribose molecules, the principal contribution to V_{NB} is the repulsive interaction between the eclipsed proton and hydroxyl attached to the $C_{2'}$ and $C_{3'}$ atoms. Coulombic forces are negligible in both molecules. The additional contributions of V_{STR} and V_{TOR}, which are again identical with those reported for ribose in Figure 3, are found to raise the e and w potential barriers of 3′-deoxyribose by 0.7 kcal/mol but are not able to account for the observed preference for n-type puckering.

As with 2′-deoxyribose, the gauche term in 3′-deoxyribose reflects the decided puckering preference of the ring. In contrast to 2′-deoxyribose, however, the gauche contribution in the 3′-deoxyribose system assumes its minimum in the n domain and its maximum in the s. The $O_{1'}$–$C_{1'}$–$C_{2'}$–$O_{2'}$ sequence, which is gauche in the n range and trans in the s quadrant, dominates the V_G term in Figure 5. The gauche interactions in the e quadrant also provide an important contribution to the energy barrier opposing the free pseudorotation of 3′-deoxyribose.

2′-Fluoro-2′-deoxyribose. The marked tendency of 2′-fluoro-2′-deoxyribose sugars to adopt n-puckered states in solid-state[58] and solution[59–61] studies can also be reconciled on the basis of the

(52) J. J. Fox, K. A. Watanabe, and A. Bloch, *Prog. Nucleic Acid Res. Mol. Biol.*, **5**, 251–313 (1966).
(53) R. J. Suhadolnik, "Nucleoside Antibiotics", Wiley-Interscience, New York, 1970.
(54) P. O. P. Ts'o in "Basic Principles in Nucleic Acid Chemistry", Vol. 1, P. O. P. Ts'o, Ed., Academic Press, New York, 1974, pp 453–584.
(55) R. A. Jones, Ph.D. Thesis, University of Alberta, Edmonton, Alberta, Canada, 1974.
(56) E. Westhof, H. Plach, I. Cuno, H.-D. Lüdemann, *Nucleic Acids Res.*, **4**, 939–954 (1977).
(57) M. M. Radwan and H. R. Wilson, *Acta. Crystallogr., Sect. B*, **B36**, 2185–2187 (1980).
(58) D. Suck, W. Saenger, P. Main, G. Germain, J.-P. Declercq, *Biochim. Biophys. Acta*, **361**, 257–265 (1974).
(59) R. J. Cushley, J. F. Codington, and J. J. Fox, *Can. J. Chem.*, **34**, 1131–1140 (1968).
(60) S. Uesugi, H. Miki, M. Ikehara, H. Iwahashi, and Y. Kyogoku, *Tetrahedron Lett.*, **42**, 4073–4076 (1979).
(61) W. Guschlbauer and K. Jankowski, *Nucleic Acids Res.*, **8**, 1421–1433 (1980).

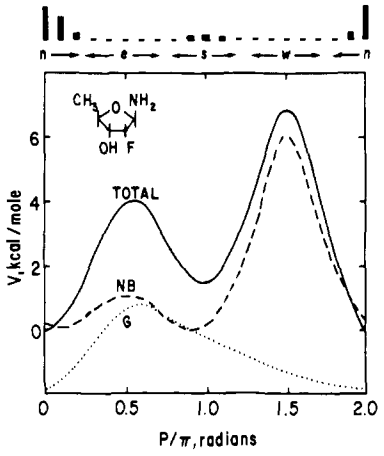

Figure 6. Variation of the total and constituent (nonbonded and gauche) energies in kcal/mol as a function of the pseudorotation of 2′-fluoro-2′-deoxyribose. See legend to Figure 3.

present potential energy calculations. According to Figure 6, the n quadrant of pseudorotation space with $\sigma_n = 0.90$ is favored almost exclusively in our 2′-fluoro model. The remainder of the population is confined principally to the s domain ($\sigma_s = 0.09$), the computed energy barrier of the intermediate e domain being almost 4 kcal/mol and that of the w domain almost 7 kcal/mol. Compared to ribose, the n–e–s path of pseudorotation of 2′-fluoro-2′-deoxyribose is somewhat more hindered and the s–w–n route slightly less hindered.

As expected, the smaller fluorine atom at $C_{2'}$ engenders fewer steric contacts and, accordingly, lesser nonbonded forces than the 2′-hydroxyl of ribose. For example, in Figure 6 the potential energy barrier at $P = 0.5\pi$ rad is only 1.1 kcal/mol compared to a value of 2.4 kcal/mol in ribose. Unlike the situation in ribose, the n and s conformers are not equally favored on the basis of V_{NB}. Indeed, the s conformers with less severe steric contacts are slightly preferred (by 0.1 kcal/mol) over the n conformers of 2′-fluoro-2′-deoxyribose. Coulombic interactions, however, are almost identical in the n- and s-puckered domains. Furthermore, the n/s preference is not altered by the V_{STR} and V_{TOR} energy terms which are identical with those of ribose.

The gauche interactions of the 2′-fluoro system are dominated by the two F–C–C–O sequences in the molecule. The V_G contribution in Figure 6 is minimized at $P = 0$ rad when the $O_{1'}$–$C_{1'}$–$C_{2'}$–$F_{2'}$ torsion is gauche and the $F_{2'}$–$C_{2'}$–$C_{3'}$–$O_{3'}$ angle is displaced from the eclipsed cis conformation. The occurrence of a trans arrangement of the $O_{3'}$–$C_{3'}$–$C_{4'}$–$O_{1'}$ sequence in this state is masked by the very large barrier governing the F–C–C–O t/g energy difference. The maximum gauche contribution for 2′-fluoro-2′-deoxyribose is located in the e quadrant where $O_{1'}$–$C_{1'}$–$C_{2'}$–$F_{2'}$ is trans and $F_{2'}$–$C_{2'}$–$C_{3'}$–$O_{3'}$ cis. According to Figure 6, the n conformer is favored over the s conformer by 1.5 kcal/mol on the basis of V_G. In addition, V_G is a major determinant of the potential energy barrier that opposes the free pseudorotation of 2′-fluoro-2′-deoxyribose through the e quadrant of puckered states.

NMR Solution Properties

The conformational energy calculations described above may be additionally tested for their ability to reproduce the three-bond proton coupling constants observed in NMR studies of the furanose in solution. Mean coupling constants determined with eq 1-6 on the basis of the above energies are compared with experimental data in Table III. The different couplings in ribose and 2′-deoxyribose are assigned the pseudorotational dependences given in Figures 2–4 of 1. The $J_{2'3''}$ and $J_{3''4'}$ proton coupling in 3′-deoxyribose are assumed to mirror the $J_{2''3'}$ and $J_{1'2''}$ couplings in 2′-deoxyribose, respectively, such that for any chosen state P, $J_{2'3''}(P) = J_{2''3'}(\pi - P)$ and $J_{3''4'}(P) = J_{1'2''}(\pi - P)$. In other words, the variations of the 3′-deoxyribose $J_{2'3''}$ and $J_{3''4'}$ are identical with those given in Figure 1–4 for the 2′-deoxyribose $J_{2''3'}$ and $J_{1'2''}$ with each value of P in the figure replaced by $\pi - P$. The 3″-proton of 3′-deoxyribose is located at position W with X = OH in Figure 1 while the 2″-proton of 2′-deoxyribose is found at position X and W = OH. The $J_{2'3'}$ coupling in 3′-deoxyribose is derived by using symmetry arguments from the relationship of Figure 1-3 with the 3′-$J_{2'3'}(P)$ equal to the 2′-$J_{2'3'}(P + \pi)$. Similarly, the 3′-deoxyribose $J_{1'2'}(P)$ and $J_{3'4'}(P)$ values are taken from Figure 1–2 as the 2′-deoxyribose $J_{1'2'}(P) - 1$ Hz and $J_{3'4'}(P) + 1$ Hz, respectively. For simplicity, the three proton coupling constants of 2′-fluoro-2′-deoxyribose are assumed to follow the same pseudorotational variations as those given in 1 for ribose.

Table III. Comparison of Theoretical Proton Coupling Constants (Hz) with Experimental Measurements

coupling const	theory	expt
	Ribose[a]	
$J_{1'2'}$	4.9	4.5 ± 1.5
$J_{2'3'}$	5.2	5.2 ± 0.2
$J_{3'4'}$	4.8	5.0 ∓ 1.5
	2′-Deoxyribose[a]	
$J_{1'2'}$	9.0	7.4 ± 0.5
$J_{1'2''}$	6.4	6.5 ± 0.5
$J_{2'3'}$	7.0	6.5 ± 0.5
$J_{2''3'}$	2.9	3.3 ± 0.5
$J_{3'4'}$	2.3	3.1 ∓ 0.5
	3′-Deoxyribose[55–57]	
$J_{1'2'}$	2.6	2.1 ± 0.4
$J_{2'3'}$	7.0	5.8 ± 0.3
$J_{2'3''}$	3.5	2.7 ± 0.4
$J_{3'4'}$	8.7	8.8 ± 1.1
$J_{3''4'}$	6.5	5.9 ± 0.1
	2′-Fluoro-2′-deoxyribose[59–61]	
$J_{1'2'}$	0.9	2.3 ± 1.1
$J_{2'3'}$	4.9	4.7 ± 0.6
$J_{3'4'}$	8.9	7.4 ± 1.9

[a] See data presented in 1.

As evident from Table III, the agreement between theoretical predictions and observed proton coupling constants is remarkably good. The above energy computations are able to account for the very distinct solution properties of four different furanose moieties. Until now, no theoretical study has been successful in reproducting the experimental descriptions of both ribose and 2′-deoxyribose sugars, let alone those of the unusual 3′-deoxyribose and 2′-fluoro-2′-deoxyribose systems. According to Table III, the observed ribose data are matched as well by the present calculations as by previous energy estimates (cf. Table III of 1). The agreement between 2′-deoxyribose observations and calculations in this work, however, is much better than earlier studies (cf. Table IV of 1). The improvement offered here is due primarily to the correctly predicted preference for s-type puckering together with the estimated ~2-kcal/mol e-type pseudorotational energy barrier. At most, only one of these features is found in other studies of 2′-deoxyribose pseudorotation. Interestingly, the numerical agreement between the theoretical and observed couplings of 3′-deoxyribose is closer than that of 2′-deoxyribose. The largest deviation in the 3′-deoxyribose data is found in the 1.2 Hz overestimate of $J_{2'3'}$. The four remaining constants are matched within 0.8 Hz by present theory. The quantitative agreement between observed and calculated proton coupling constants is somewhat less satisfactory for 2′-fluoro-2′-deoxyribose. The 1.4- and 1.5-Hz discrepancies in $J_{1'2'}$ and $J_{3'4'}$, respectively, may be somewhat improved if electronegatively effects of the 2′-fluorine are included in the computations. The present approach is, nevertheless, clearly successful in its correct prediction of $J_{3'4'}$ to exceed $J_{1'2'}$ in 2′-fluoro-2′-deoxyribose.

Geometric Fluctuations

The extent to which fluctuations of the pentose geometry away from standard X-ray values influence the computed potential energy of pseudorotation is illustrated in Figure 7. In this example the nonbonded contributions to the total energy of 2′-deoxyribose

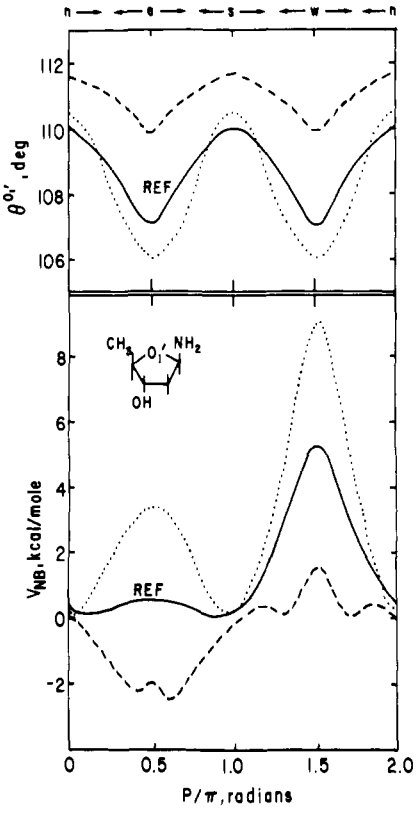

Figure 7. Computed dependence of the pseudorotational energy of 2′-deoxyribose as a function of the internal geometry of the ring. The endocyclic valence angle centered at $O_{1'}$ ($\theta^{O_{1'}}$) and the associated nonbonded potential energy are reported for three different cycles of pseudorotation, each with $\tau_m = 38°$. Refer to text for additional details.

are plotted (on a relative scale) as a function of the pseudorotational phase angle for three different sets of interconverting pentose rings. Each set of structures is also characterized by the sequential variations of the endocyclic C_4–O_1–$C_{1'}$ valence angle ($\theta^{O_{1'}}$) along its $\tau_m = 38°$ pseudorotational path. For the sake of clarity, the various changes in the four remaining valence angles of the three puckering sequences are omitted from the figure. The $\theta^{O_{1'}}$ values and V_{NB} contributions associated with the energetically optimized ring structures of the present study are illustrated by the two solid curves labeled REF (for reference). These data are taken from Figures 2 and 4, respectively. A more opened set of ring structures characterized by larger values of $\theta^{O_{1'}}$ compared to the REF data is described by the pair of dashed curves in Figure 7, while a more compact set of structures with $\theta^{O_{1'}}$ angles generally smaller than REF values is represented by the pair of dotted curves.

The computed dependence of the nonbonded pseudorotational potential energy upon the different ring geometries is striking. Apparently minor 2–3° fluctuations of valence angles describe dramatically different pseudorotational behavior. A series of small increases in $\theta^{O_{1'}}$ over the entire pseudorotation cycle, for example, introduces a dip in the usual nonbonded potential energy barrier of 2′-deoxyribose at $P = 0.5\pi$ rad (dashed curves). This unusual minimum presumably reflects the very large distance of separation between the heavy-atom side groups attached to the $C_{1'}$ and $C_{4'}$ atoms of the e-puckered ring. The interactions between the $C_{1'}$ and $C_{4'}$ side groups, however, assume more importance in ring structures closer to standard X-ray geometries. The V_{NB} minimum at $P = 0.5\pi$ rad changes to a local maximum as $\theta^{O_{1'}}$ decreases, and the $C_{1'}$ and $C_{4'}$ side groups move closer together. Indeed, if $\theta^{O_{1'}}$ contracts to 106°, the e-puckering nonbonded energy barrier rises to nearly 3.5 kcal/mol in height. The local energy maximum at $P = 1.5\pi$ rad also increases in magnitude as the $\theta^{O_{1'}}$ angle decreases in value.

The remaining contributions to the total potential energy exhibit little, if any, dependence upon the slight perturbations of ring geometry illustrated in Figure 7. Nevertheless, as a consequence of the geometric influence upon nonbonded interactions, the theoretical description of 2′-deoxyribose pseudorotation can range from a freely rotating to a severely restricted sequence of puckerings in the above examples. The repulsive torsional and gauche potential energy contributions at $P = 0.5\pi$ rad (cf. Figure 4), for example, cancel the local nonbonded energy minimum in Figure 7 associated with "open" ring geometries so that the total energy is nearly constant between $P = 0$ and π rad. The same repulsive terms, however, add to the nonbonded energy barriers favored in "compact" rings where $\theta^{O_{1'}}$ is small so that the total pseudorotational potential at 0.5π rad reaches 5 kcal/mol. The significant discrepancies among various theoretical estimates of the pseudorotational energy outlined in 1 may very likely reflect the features of ring geometry introduced in the different calculations. Interestingly, structures that resemble the limited X-ray examples encounter hindered, rather than free, pseudorotation.

Summary

The potential energy calculations outlined here offer several new clues to the nature of furanose pseudorotation. The results not only confirm the hindered ring flexibilities suggested by solid-state and solution studies of low molecular weight nucleic acid analogues but also suggest a structural rationale behind the observed properties. The distinct differences in the pseudorotation of ribose and 2′-deoxyribose, for example, apparently stem from the unique combinations of nonbonded forces and gauche interactions associated with the two sugars. The opposing contributions of valence angle strain and torsion angle deformation to the total potential energy essentially cancel one another in both systems so that no conformers predominate on these grounds. Favorable steric interactions combined with the strong tendencies of the O–C–C–O bond sequences to adopt gauche rotational arrangements thus induce the ribose to adopt n- or s-type puckerings. Substitution of the 2′-hydroxyl of ribose by a proton in 2′-deoxyribose, however, introduces a strong imbalance in the gauche interactions that determine the 50:50 blend of n/s ring (e.g., ribose) puckerings. The single O–C–C–O sequence in 2′-deoxyribose pushes the n/s equilibrium firmly into the direction of s puckering. The less severe nonbonded contacts engendered by the proton in 2′-deoxyribose additionally lower the potential energy barrier opposing "free" pseudorotation. Unfavorable gauche interactions, nevertheless, continue to oppose completely unrestricted motion of the 2′-deoxyribose sugar.

The faithful correspondence of theory with observations clearly enhances the predictive value of our theoretical approach in general. Potential functions introduced to treat common ribose and 2′-deoxyribose analogues account as well for the properties of less common 3′-deoxyribose and 2′-fluoro-2′-deoxyribose rings. Analyses currently in progress likewise confirm the experimental behavior of arabinose, xylose, and lyxose systems in dilute solution. In all cases considered to date, gauche effects appear to be a major determinant of ring puckering. Furthermore, only the gauche contributions provide a satisifactory rationale behind the observed pseudorotational motions of 2′-deoxyribose, 3′-deoxyribose, and 2′-fluoro-2′-deoxyribose. The importance of gauche factors in these calculations also clarifies arguments introduced elsewhere[61] to explain furanose pseudorotational behavior on the basis of atomic electronegativities. The gauche effect reflects bond–antibond orbital interactions between vicinal polar bonds[17] while electronegativities measure the degree of polarity of these bonds. Increases in bond polarity presumably enhance the proclivity of a three-bond sequence to adopt gauche conformations.

The success of the above computations depends as well upon the direct geometric approach introduced here to describe sugar puckering. This procedure helps to guarantee that the resulting geometries of the puckered rings conform to the bond length and valence angle restraints of X-ray crystallographic examples. Minor deviations from standard geometries can alter the computed potential energies of pseudorotation drastically.

Finally, the correspondence of the very simple chemical models used in this calculation with the pseudorotational behavior of more complicated nucleosides and nucleotides suggests the limited in-

fluences of base type upon ring puckering, at least for the more common systems. Altona and co-workers have recently reached similar conclusions through analyses of the β-D-furanoside fragments of various X-ray crystal structures.[62]

Acknowledgment. The author is grateful to the National Institute of Health (USPHS Grant GM-20861) and to the Charles and Johanna Busch Memorial Fund of Rutgers University for laboratory support, to Professor Joachim Seelig for his hospitality at the Biozentrum of the University of Basel, Switzerland, where this work was initiated, to the J. S. Guggenheim Memorial Foundation for a fellowship, to the University of Basel Computer Center and the Center for Computer and Information Services of Rutgers University for computer time, and to the USPHS for a Research Career Development Award (Grant GM-00155).

Registry No. Ribose, 79681-15-5; 2′-deoxyribose, 79681-16-6; 3′-deoxyribose, 79681-17-7; 2′-*F*-2′-deoxyribose, 79681-18-8.

Supplementary Material Available: Pseudorotation coordinates of ribose (Table I-S) (2 pages). Ordering information is given on any current masthead page.

(62) H. P. M. de Leeuw, C. A. G. Haasnoot, and C. Altona, *Isr. J. Chem.*, **20**, 108-126 (1980).

Communications to the Editor

Small Ring Heterocycles. Role of Azabenzvalenes in the Thermolysis of 3-Cyclopropenyl Substituted Oxazolinones

Albert Padwa,*† Mitsuo Akiba, Leslie A. Cohen, Henry L. Gingrich,‡ and Nobumasa Kamigata

Department of Chemistry, Emory University Atlanta, Georgia 30322

Received August 3, 1981

The rearrangement of 3,3′-bicyclopropenyls to benzene derivatives is one of the most exothermic unimolecular isomerizations known.[1-8] Its mechanism has been a source of controversy over the years. At various times the rearrangement has been postulated to proceed through Dewar benzene,[3] benzvalene,[9] prismane,[1] diradical[6] and ionic intermediates.[3] The most recent data are consistent with a path involving initial homolytic cleavage of one of the cyclopropene rings followed by expansion of the other ring, closure to a Dewar benzene, and finally opening of the Dewar intermediate to form aromatic products.[7,8] The conversion of the closely related 3-azirinylcyclopropene system (**1**) to a pyridine derivative **4** represents a more complicated transformation since several different possibilities are available. One of the more attractive paths involves the initial formation of a nitrile ylide intermediate[10] **2** followed by intramolecular dipolar cycloaddition[11] to give azabenzvalene (**3**) which subsequently rearranges to pyridine (**4**). In this communication we report the results of our investigations dealing with the conversion of cyclopropenyl substituted nitrile ylides to pyridines according to the mechanism outlined in Scheme I.

Scheme I

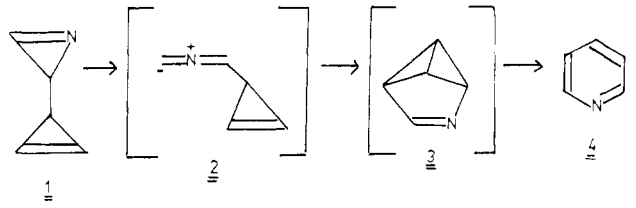

Scheme II

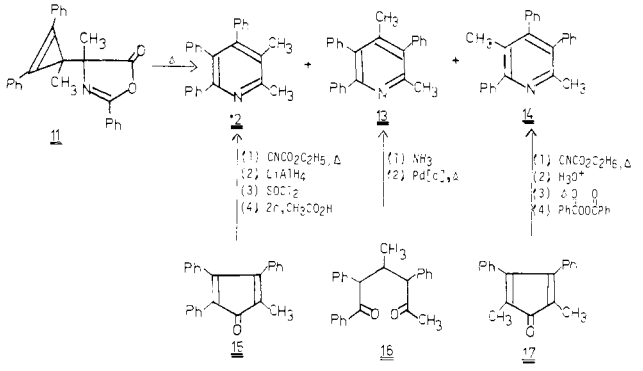

Thermolysis or photolysis of a sample of the 3-cyclopropenyl-substituted 2*H*-azirine **5**[12] produced 2-methyl-3,4,5,6-tetraphenylpyridine (**6**),[13] mp 160-161 °C, in quantitative yield.

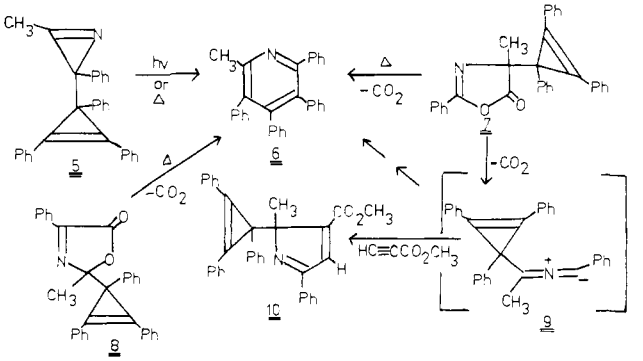

We believe that the rearrangement of **5** to **6** occurs via the se-

† John S. Simon Guggenheim Memorial Fellow, 1981-1982.

‡ Agricultural Chemical Research Group, FMC Corporation, Princeton, New Jersey 08540.

(1) Breslow, R.; Gal, P.; Chang, H. W.; Altman, L. J. *J. Am. Chem. Soc.* **1965**, *87*, 5139.

(2) Weiss, R.; Kempeke, H. P. *Tetrahedron Lett.* **1974**, 155.

(3) Weiss, R.; Andrae, S. *Angew. Chem.* **1973**, *85*, 145, 147; *Angew Chem., Int. Ed. Engl.* **1973**, *12*, 150, 152.

(4) DeWolf, W. H.; Stol, W.; Landheer, I. J.; Bickelhaupt, F. *Recl. Trav. Chim. Pays-Bas.* **1971**, *90*, 405.

(5) DeWolf, W. H.; Landheer, I. J.; Bickelhaupt, F. *Tetrahedron Lett.* **1975**, 179.

(6) Weiss, R.; Kobl, H., *J. Am. Chem. Soc.* **1975**, *97*, 3222, 3224.

(7) Davis, J. H.; Shea, K.; Bergman, R. G. *Angew. Chem., Int. Ed. Engl.* **1976**, *15*, 232. *J. Am. Chem. Soc.* **1977**, *99*, 1499.

(8) Turro, N. J.; Schuster, G. B.; Bergman, R. G.; Shea, K. J.; Davis, J. H. *J. Am. Chem. Soc.* **1975**, *97*, 4758.

(9) Landheer, I. J.; DeWolf, W. H.; Bickelhaupt, F. *Tetrahedron Lett.* **1975**, 349; **1974**, 2813.

(10) Padwa, A. *Acc. Chem. Res.* **1976**, *9*, 371.

(11) For leading references of intramolecular cycloadditions of nitrile ylides, see: Padwa, A.; Ku, A.; Carlsen, P. H. J. *J. Am. Chem. Soc.* **1978**, *100*, 3494.

(12) 2*H*-Azirine **5** was prepared by treating triphenylcyclopropenyl perchlorate with the anion derived from phenylacetone *N,N*-dimethylhydrazone followed by quaternarization with methyl iodide and treatment with sodium isopropoxide. Complete details will be provided in a later publication.

(13) Wakatsuki, Y.; Yamazaki, H. *Tetrahedron Lett.* **1973**, 3383.

0002-7863/82/1504-0286$01.25/0